

## Development of a three-dimensional valence-band structure in Ag overlayers on Cu(001)

J. G. Tobin,\* S. W. Robey,<sup>†</sup> L. E. Klebanoff,<sup>‡</sup> and D. A. Shirley

*Materials and Molecular Research Division, Lawrence Berkeley Laboratory, Berkeley, California 94720  
and Departments of Chemistry and Physics, University of California, Berkeley, California 94720*

(Received 11 August 1986; revised manuscript received 29 January 1987)

Using monochromatic synchrotron radiation over the energy range of 6–32 eV, the development of the valence-band electronic structure of Ag overlayers on Cu(001) was followed with angle-resolved photoelectron spectroscopy. The *d*-band electronic structure was observed to be two dimensional for a single adlayer of  $c(10\times 2)\text{Ag}/\text{Cu}(001)$ . With five layers of coverage, the silver valence-band structure was bulklike, three-dimensional, and very similar to that of Ag(111).

### I. INTRODUCTION

Over the last several years, a number of photoemission experiments and calculations have investigated the properties of metal-overlayer–metal-substrate systems.<sup>1</sup> In particular, experimental<sup>2</sup> and theoretical<sup>3</sup> efforts have been made to elucidate the effect of thickness upon the electronic structure of thin metal slabs. An earlier Communication<sup>4</sup> gave a brief report of the development from two-dimensional to three-dimensional valence electronic structure in the silver overlayer of the all-metal system  $c(10\times 2)\text{Ag}/\text{Cu}(001)$ . A full report of the two-dimensional silver valence-band structure at monolayer coverages was presented in Ref. 1. In this paper, we present a more complete discussion of the angle-resolved photoemission experiment at higher exposures. This synchrotron-radiation based study documents the development of the electronic structure in the overlayer from two-dimensional to three-dimensional bulk behavior.

The system  $c(10\times 2)\text{Ag}/\text{Cu}(001)$  was chosen for several reasons, including its layer-by-layer growth pattern at low coverages and the expectation that this would continue at higher exposures, the ease of preparation, the stability of its constituents *in vacuo*, the limited overlap in energy of the valence bands of adsorbate and substrate, and the fact that Ag(111) has been studied in detail.<sup>1,5</sup> This system also has the distinct advantage of commensurate but nonepitaxial growth: low-energy electron diffraction (LEED) as well as Auger electron spectroscopy (AES) can therefore be used to follow the growth pattern. The overlayer of the  $c(10\times 2)\text{Ag}/\text{Cu}(001)$  system has a slightly strained hexagonal geometrical structure. It seemed reasonable to expect that at higher coverages it would approach the geometrical and electronic structure of the (111) face of crystalline silver. This behavior was in fact observed at the rather low coverage of 5 monolayers (ML).

The remainder of this paper is organized as follows: Section II is a description of the experimental details, Sec. III contains photoemission results, and Sec. IV is a discussion of those results. Section V contains a summary of conclusions.

### II. EXPERIMENTAL PROCEDURE

The first part of this section is devoted to the details of the photoemission experiments. The second part deals

with the LEED and AES calibration performed to allow accurate and reproducible preparation of evaporated samples.

#### A. The photoemission experiments

The measurements were made at the Stanford Synchrotron Radiation Laboratory (SSRL) on beam line I-2, over the energy range of  $h\nu=6\text{--}32$  eV, with an angle-resolved photoelectron (ARP) spectrometer described previously.<sup>6</sup> The base pressure during the experiment was  $1\times 10^{-9}$  Torr and operation of the Ag evaporator had essentially no effect upon the chamber pressure. Fortunately, Ag and Cu metal surfaces are both relatively nonreactive and thus less susceptible to contamination. Spectra taken at SSRL under these conditions were consistent with those collected in-house using He I and Ne I lamp sources, in a superior vacuum environment (base pressure of  $2\times 10^{-10}$  Torr).<sup>1</sup>

The Cu(001) crystal was cut and polished to within  $\pm 1^\circ$  of the (001) face and chemically polished before introduction into the vacuum system. The crystal was aligned *in situ* using LEED and laser autocollimation to a precision of better than  $\pm 1^\circ$ . The crystal had a specular finish and sharp  $1\times 1$  LEED spots, indicative of surface ordering. Evaporations were performed using a thermal source of Ag atoms which was monitored with a quartz-crystal microbalance. The source and microbalance were contained inside a shielded assembly with a shutter to allow time-controlled evaporations.

Room-temperature Ar-ion etching at pressures of  $10^{-5}$  Torr was used to remove evaporated Ag, monitored by Auger spectroscopy, but cycles of heating to between 500 and 600°C and cooling with continuous sputtering were used to remove residual contaminants. A final annealing to above 500°C was used to order the clean Cu(001) crystal, at which point contaminant levels were such that neither oxygen nor sulfur was detectable and the  $I_{\text{C}}/I_{\text{Cu}}$  Auger intensity ratio was 0.004—all measured using a four-grid LEED system in a retarding-field mode.

Possible sulfur impurities were detected at lower exposures but after extended photoemission measurements and all evaporations, the sulfur and oxygen impurities were barely detectable. Any possible carbon Auger line was obscured by an Auger line of Ag at 260 eV.

TABLE I. This is a summary of the observed and predicted Ag-to-Cu photoemission intensity ratios and the ratio of the experimental to theoretical values,  $\mathcal{R}$  [=expt/(theor)]. They are normalized to the 1-ML value, such that  $R'_n = R_n/R_1$  with  $R_n = (j_{\text{Ag}}/i_{\text{Cu}})_n$ . The subscript  $n$  represents the exposure in ML. The thickness of a monolayer is defined as  $t$  and assumed to be approximately 2.5 Å. The escape depth of an electron of a given kinetic energy is  $z_0$ . These were taken from the "Universal Curve" of electron escape depths (Ref. 20). The Appendix has a derivation of the attenuation model.

$h\nu$ (eV)	$z_0$ (Å)	$t/z_0$		$R'_1$	$R'_2$	$R'_3$	$R'_4$	$R'_5$	Average $\pm$ standard deviation
16	15	$\frac{1}{6}$	Expt.	1	2.9	3.9	4.6	6.3	
			Theor.	1	2.2	3.6	5.2	7.2	
			$\mathcal{R}$		1.3	1.1	0.9	0.9	1.0 $\pm$ 0.2
21	10	$\frac{1}{4}$	Expt.	1	2.9	4.7	5.5	8.7	
			Theor.	1	2.3	3.9	6.0	8.8	
			$\mathcal{R}$		1.3	1.2	0.9	1.0	1.1 $\pm$ 0.2
32	7.5	$\frac{1}{3}$	Expt.	1	3.6	6.2	5.2	7.4	
			Theor.	1	2.4	4.3	7.1	10.9	
	5	$\frac{1}{2}$	Theor.	1	2.6	5.4	9.8	17.2	
			$\mathcal{R}$		1.4	1.1	0.5	0.4	0.85 $\pm$ 0.5

The analyzer resolution was kept at 60 meV (10-eV pass energy) throughout the experiment, but the monochromator contribution varied with photon energy and slit width.<sup>7</sup> It is assumed that the full width at half maximum (FWHM) linewidths add in quadrature. For 6 eV  $\leq h\nu \leq 24$  eV, 65 meV  $\leq \Delta E$  (FWHM)  $< 100$  meV. For  $h\nu = 26$  eV,  $\Delta E = 111$  meV;  $h\nu = 28$  eV,  $\Delta E = 169$  meV;

$h\nu = 30$  eV,  $\Delta E = 191$  meV;  $h\nu = 32$  eV,  $\Delta E = 215$  meV. The half-angular acceptance of the electrostatic analyzer was always  $\pm 3^\circ$  or less.

All the photoemission spectra were taken with  $p$ -polarized radiation, usually at normal emission. The polarization was in the horizontal plane, as were the Poynting vector of the light, the surface normal, and the (110) plane of Cu(001). The angle of incidence of the light was  $60^\circ$  with respect to the normal. The single domain<sup>1</sup> of the  $c(10 \times 2)\text{Ag}$  was oriented such that the polarization and the  $\bar{\Gamma}-\bar{\Sigma}-\bar{M}$  direction of the hexagonal surface Brillouin zone were in the same plane, as shown in Fig. 1.

The binding energies ( $B^F$ ) were measured with respect to the Fermi energy ( $E_F$ ), which was determined separately in each individual spectrum as the point of maximum slope in the rise from background to the initial  $s$ - $p$  plateau or band feature. The position or the Fermi edge was highly reproducible, over all coverages and photon energies.<sup>7</sup> The rms scatter in its determination was typically less than 30 meV.

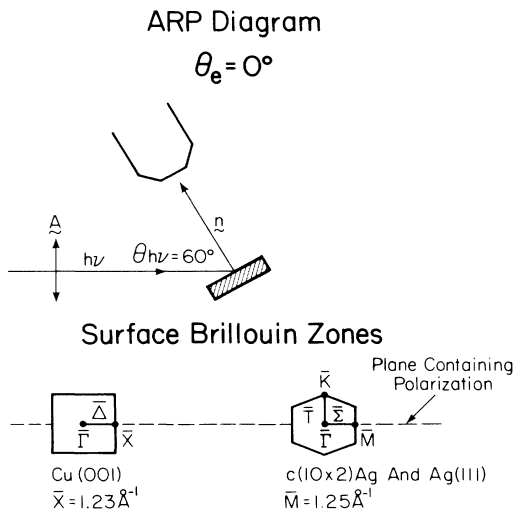


FIG. 1. The geometry of the photoemission experiment is illustrated here. Top—the real-space relationships; bottom—the surface Brillouin zones in reciprocal space and their relationships to the plane containing the polarization  $\mathbf{A}$ . The surface normal,  $\mathbf{n}$ , the light polarization, and the Poynting vector of the light are all in the horizontal plane.

## B. LEED and AES calibration

AES and LEED were used to calibrate the quartz microbalance thickness monitor, as previously discussed in Ref. 1. In a layer-by-layer growth pattern, a discontinuity in the slope of the ratio of adsorbate to substrate intensities is to be expected at 1 ML coverage. Ratios were used because of inaccuracies introduced into absolute measurements by movement of the crystal during the experiment. At a slightly higher coverage than that corresponding to the discontinuity in the slope of the  $I_{\text{Ag}(350 \text{ eV})}/I_{\text{Cu}(60 \text{ eV})}$  intensity ratio, the first  $c(10 \times 2)$  LEED spots were observed. The quartz microbalance was thus calibrated for

subatomic and multiatomic layer coverages of Ag on the Cu(001) crystal and used as a guide during evaporations.

As a check on the accuracy of the quartz microbalance, derivative intensity measurements were made of each sample for the Auger lines of Cu *MVV* (60 eV), Ag *MNV* (350 eV), and Cu *LMM* (920 eV) and compared to the original measurements,  $I_{\text{Ag}(350 \text{ eV})}/I_{\text{Cu}(60 \text{ eV})}$  and  $I_{\text{Ag}(350 \text{ eV})}/I_{\text{Cu}(920 \text{ eV})}$ , taken during calibration. The Cu (920 eV) measurements were necessary because at higher exposures the Cu (60 eV) is drastically attenuated due to its much shorter mean free path. The results proved to be generally internally consistent. The estimate of the accuracy is typically  $\pm 20\%$  of the exposure.

LEED observations made at higher coverages (2–5 ML) showed that the pattern was remaining essentially the same as that at 1 ML, but that the adsorbate spots were increasing in number, intensity and sharpness relative to substrate spots, with a possible removal of the splitting of some of the adsorbate spots. In an earlier LEED and AES experiment,<sup>1,7</sup> it had been observed that at coverages around 10 ML the copper substrate spots were no longer visible and the adsorbate spots were qualitatively the same as those of a Ag(111)  $1 \times 1$  pattern. The normal-emission HeI photoemission spectrum collected at this exposure was very similar to that of the Ag(111) spectrum of Spears *et al.*<sup>8</sup>

Finally, the ratio of the photoemission intensities of the silver and copper valence features was used to check the results of the LEED-AES experiments. In general, they confirmed the LEED-AES results. The relative intensities of the silver and copper valence bands were normalized to that for 1 ML. An empirical function which consisted of a scaled and shifted clean copper spectrum was used to fit the residual copper features. The silver intensity was obtained by subtracting the empirical function from the spectrum and then summing the intensity of the individual channels. These results were then compared to the predictions of a simple model including attenuation effects, a description of which is in the Appendix. A summary is given in Table I. Taken all together, the ratios are reasonably consistent. However, these results must be approached with caution: the cross sections of the silver valence bands may be changing with exposure, as well as the illumination and magnitude and direction of the polarization of each layer.

As discussed in Ref. 1, this Cu(001) sample exhibited only one of the two possible orthogonal domains of the  $c(10 \times 2)$  structure. This may have been caused by the slight misalignment of ( $\pm 1^\circ$ ) the crystal face from (001) and the subsequent breakdown of the degeneracy of the [100] and [010] directions due to steps. Because of the localized sampling of the photoemission process, the presence or absence of the second domain is not crucial.

### III. PHOTOEMISSION RESULTS

Photoemission spectra were collected for photon energies in the range 6–32 eV from samples with Ag coverages between  $\frac{1}{2}$  and 5 ML and for clean Cu(001) and Ag(111).<sup>5</sup> A complete presentation of these spectra is available in Ref. 7. All copper and Ag/Cu(001) spectra in

Figs. 2–6 were collected at normal emission with the experimental geometry illustrated in Fig. 1, as were the Ag(111) (Ref. 5) spectra in Figs. 2–6. This was to facilitate the comparison of the  $c(10 \times 2)$  spectra with those of the Ag(111). It is especially important that the surface Brillouin zones of the Ag(111) and the  $c(10 \times 2)$ Ag were oriented the same with respect to the Poynting vector and polarization of the radiation. While all of the data were used in the analysis, only a few particularly representative spectra will be reproduced here.

Figure 2 shows spectra taken at  $h\nu=6, 7,$  and 8 eV. A major point of interest here is the development of a precursor to the Ag(111) surface state that occurs near  $E_F$ . This is most easily seen in the 7- and 8-eV spectra, where the silver state grows in continuously, while the copper features are slowly diminishing. Also of interest is the absence of a silver overlayer feature corresponding to band 6 in Ag(111), which is present at  $h\nu=6, 7,$  and 8 eV at  $B^F$  near 1–2 eV. This will be discussed in detail in Sec. IV.

As the photon energy is increased through our experi-

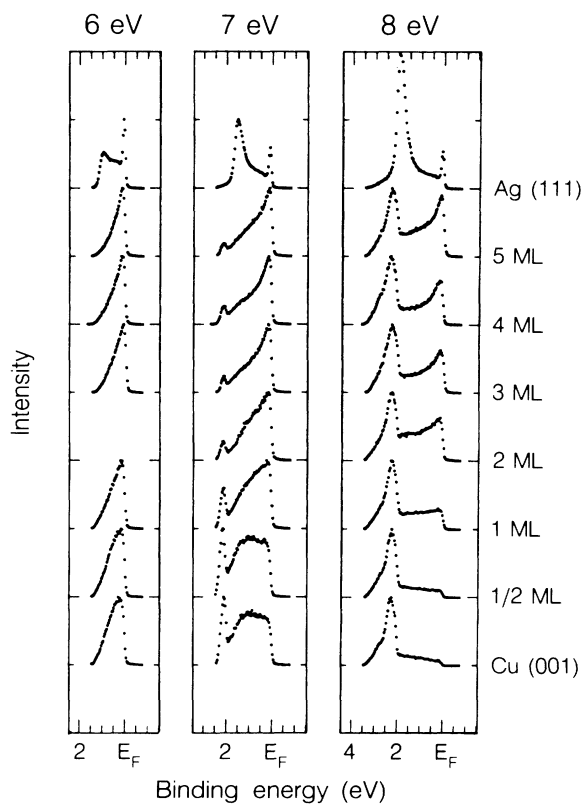


FIG. 2. The ARP spectra taken at  $h\nu=6, 7,$  and 8 eV are plotted vs the binding energy ( $B^F$ ) with respect to the Fermi level ( $E_F$ ). The spectra are normalized to the largest feature in each spectrum. Cu(001) is at the bottom, followed sequentially upward by the spectra of  $c(10 \times 2)$ Ag/Cu(001) of  $\frac{1}{2}, 1, 2, 3, 4,$  and 5 ML exposures. The bulk, single-crystal Ag(111) spectrum is topmost. All of the data was collected at normal emission, either parallel to [001] of Cu(001) or [111] of Ag(111). In the 8-eV plot, the Ag(111) spectrum was expanded to more fully illustrate the surface state near  $E_F$ .

mental range, the element of volume in  $k$  space which the photoemission process samples moves toward the centers of the three-dimensional Brillouin zones of both silver and copper. As would be expected from the known band structures of bulk Cu and Ag, the overlap of adsorbate and substrate features thereupon is observed to decrease. This is apparent in Fig. 3, where spectra taken with  $h\nu=14$  eV are shown. At  $h\nu=14$  eV, a trio of silver features near  $B^F=4.6$  eV, a shoulder, a peak, and another shoulder, are easily visible as is a weaker feature at higher coverage and binding energy, near  $B^F=5.5$  eV. The high binding energy shoulder at 4.9 eV may be a copper feature in the  $h\nu=14$ -eV spectra. At binding energies above that, peaks are not identifiable, except at the highest exposures.

For  $h\nu \geq 14$  eV, the higher exposure  $c(10 \times 2)\text{Ag}/\text{Cu}(001)$  surfaces have spectra that are very similar in appearance to the bulk Ag(111) spectra, if the copper features at lower binding energies are ignored. This is emphasized by the decreasing electron escape depth with increasing electron (and thus photon) energy, which serves to amplify the Ag-overlayer-Cu-substrate spectral intensity ratio. The absence of band 6 and hence the failure of the lower photon energy spectra of the higher exposure samples to closely mimic the Ag(111) spectra will be discussed in the next section.

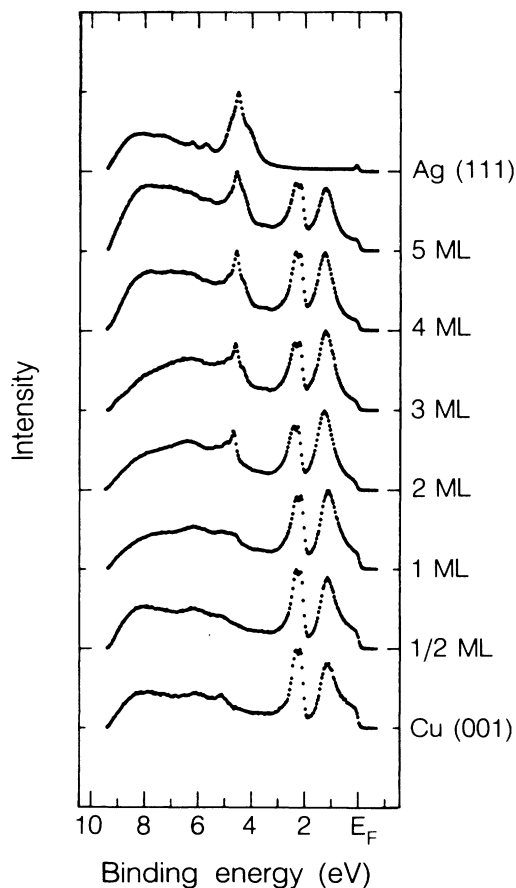


FIG. 3. Same as Fig. 2 with  $h\nu=14$  eV.

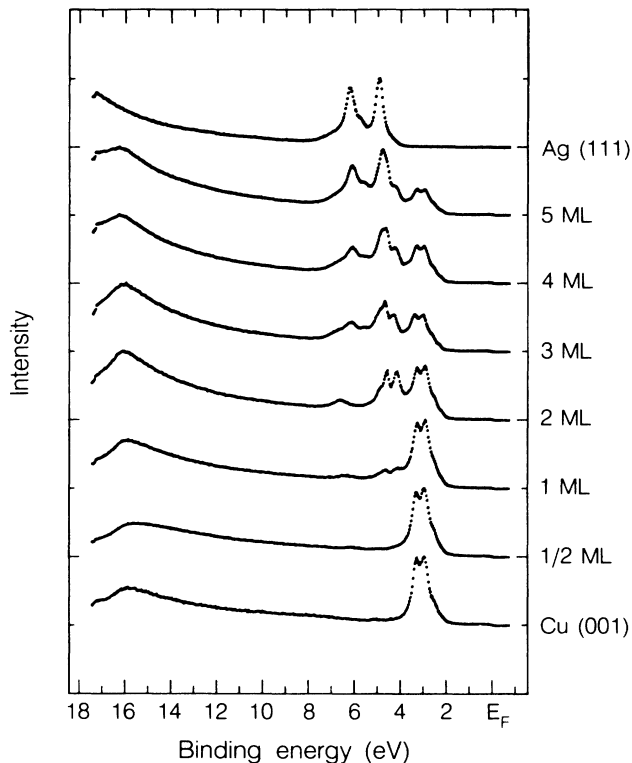


FIG. 4. Same as Fig. 2 with  $h\nu=24$  eV.

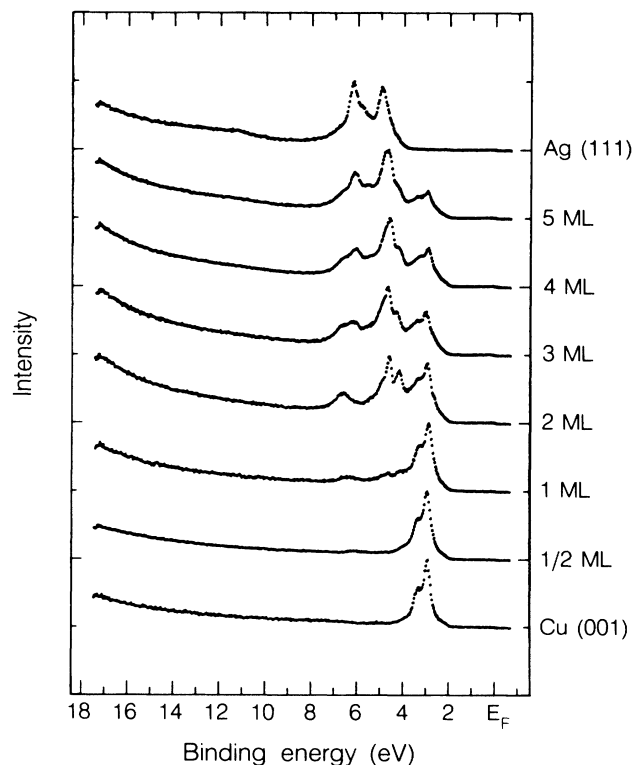


FIG. 5. Same as Fig. 2 with  $h\nu=28$  eV.

In Fig. 4, the spectra taken at  $h\nu=24$  eV are shown. The features at  $B^F=4.3, 4.7, 4.8, 5.6, 6.1,$  and  $6.9$  eV are present at photon energies of 21–24 eV, with the shoulder peak near 4.7 eV being among those most prominent. The feature at  $B^F=6.9$  eV at 5 ML is absent at  $h\nu=23$  and 24 eV, lost in the broadening tail of the other peaks. In these spectra the peak at 4.3 eV is quite strong, particularly at coverages of 2 and 3 ML of silver. It is enveloped by the broadening 4.8-eV peak at higher exposures, where it becomes a shoulder on the leading edge of the silver  $d$  bands. Also, the peaks at greater binding energies are undergoing a relative increase in intensity, particularly at exposures of 4 and 5 ML, thus mimicking the behavior of the peaks in the Ag(111) spectra. This contributes to the difficulty in observing the feature at  $B^F=6.9$  eV at 5 ML.

The spectra taken at  $h\nu=26, 28, 30,$  and  $32$  eV continue the trends observed at  $h\nu=21$ –24 eV, but the degraded resolution causes a larger sampling of  $k$  space and more averaging over the Brillouin zone. This is illustrated by the  $h\nu=28$ -eV spectra in Fig. 5. The most striking features are those at a coverage of 2 ML. As above, a strong separate peak at  $B^F=4.2$  eV is present, before it becomes a shoulder at higher exposures. Again there is a very strong resemblance between the silver overlayer features at higher exposures and the Ag(111) spectrum.

At photon energies of 26 eV and above, a broad feature is present in the Ag(111) spectra at a kinetic energy of 17 eV with respect to the Fermi level ( $B^F=h\nu-17$  eV). The highest exposure  $c(10\times 2)\text{Ag}/\text{Cu}(001)$  samples also displayed this very broad, weak peak at  $h\nu\geq 28$  eV, as indicated by the arrows in Fig. 6.

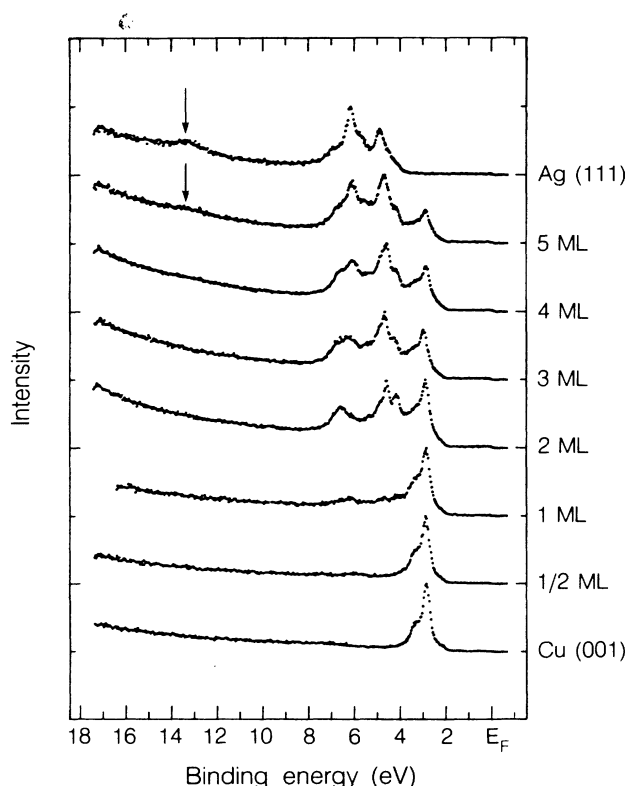


FIG. 6. Same as Fig. 2 with  $h\nu=30$  eV.

#### IV. DISCUSSION

We discuss dispersive behavior in the Ag overlayer in Sec. IV A, followed by a comparison with Ag(111) in Sec. IV B.

##### A. Dispersive behavior

The above data were collected over the range of  $h\nu=6$ –32 eV with the electron emission along the surface normal. The component of photoelectron momentum parallel to the surface is zero and the component perpendicular to the surface is equivalent to the total crystal momentum. Thus this is a direct probe of the dependence of the dispersion relations upon the perpendicular component of the crystal momentum and a test for three dimensionality in the valence-band dispersion. Energy conservation can be expressed in the following form:

$$B^F = h\nu - E_{\text{kin}} - \varphi, \quad (1)$$

with  $E_{\text{kin}}$  the kinetic energy,  $h\nu$  the photon energy,  $B^F$  the binding energy with respect to the Fermi level, and  $\varphi$  the work function of the crystal.

For normal emission from Ag(111), the final state is a particularly well-defined, single state.<sup>5</sup> The final state of the photoelectrons emitted from the  $c(10\times 2)\text{Ag}$  adlayers is not well understood. To avoid any unnecessary and possibly prejudicial assumptions concerning the final state, the comparison of the overlayer and Ag(111) dispersion relations will be made empirically by plotting the binding energies versus photon energy. Figures 7–11 are plots of the  $B^F$  values of the silver features versus photon

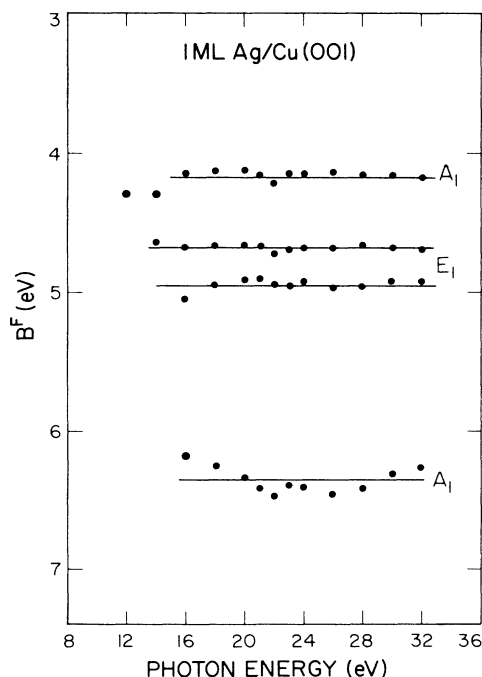


FIG. 7. This is a plot of the binding energy ( $B^F$ ) with respect to the Fermi level ( $E_F$ ) of the silver overlayer features at 1-ML exposure vs the photon energy.

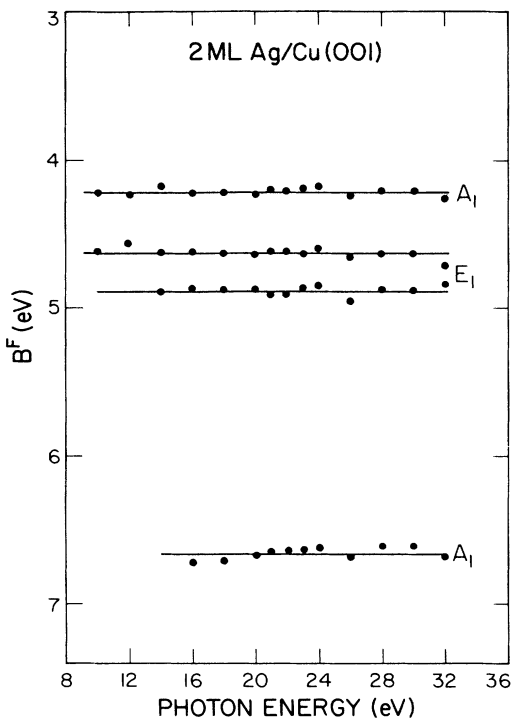


FIG. 8. Same as Fig. 7 but for an exposure of 2 ML.

energy for 1, 2, 3, 4, and 5 ML coverages, respectively. Figure 12 is a plot of the Ag(111) data versus photon energy. With respect to Figs. 7–11, separating the silver adsorbate from the copper substrate features was sometimes difficult. Any silver feature overlapping with the strong copper  $d$ -band peaks near  $B^F=2-3$  eV was essentially

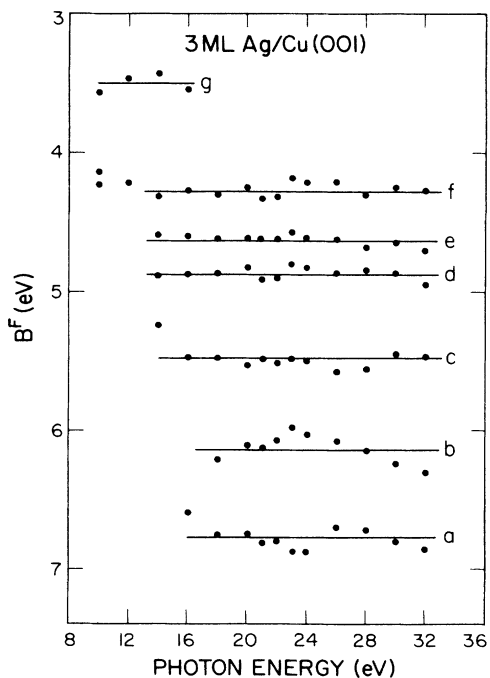


FIG. 9. Same as Fig. 7 but for an exposure of 3 ML.

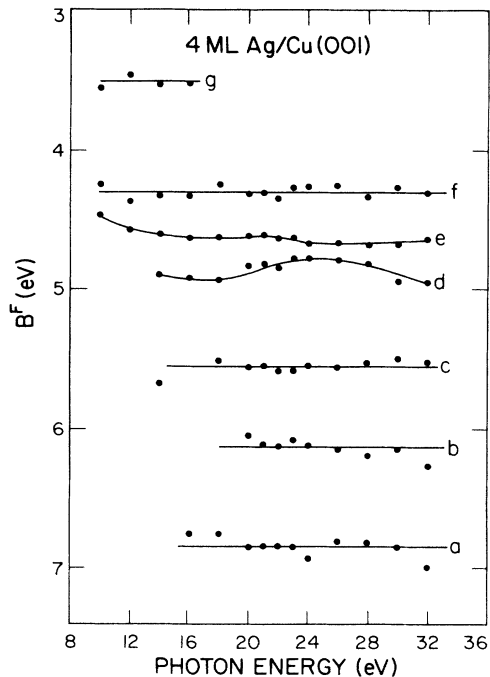


FIG. 10. Same as Fig. 7 but for an exposure of 4 ML.

lost. On the other extreme, the weak copper feature at  $B^F \geq 5$  eV caused significant problems in assignment of weak peaks and shoulders in the region. Nevertheless, the high energy and angular resolutions used made peak assignment possible.

A careful examination of the binding energies ( $B^F$ )

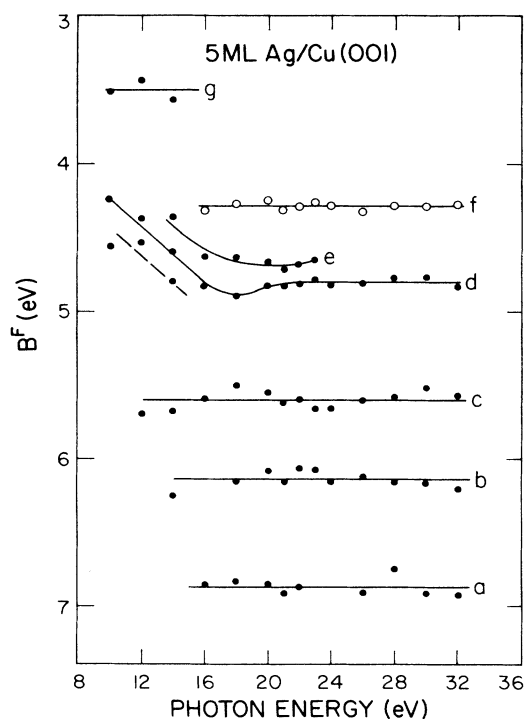


FIG. 11. Same as Fig. 7 but for an exposure of 5 ML.

with respect to the Fermi level shows marked changes in going from 1 to 2 to 3 ML and demonstrates a convergence toward Ag(111)-like behavior at coverages of 4 and 5 ML. Each of the lower coverages will be discussed separately.

*One monolayer.* At 1-ML coverage, the geometrical structure of the adlayer is known to be an atomic monolayer film and the  $d$ -band electronic structure of the adlayer has been shown to be primarily two-dimensional.<sup>1</sup> In Fig. 7, the silver features of the 1-ML coverage sample are shown *not to disperse* with photon energy and are thus independent of  $k_{\perp}$ , the perpendicular component of momentum. The scatter in the points simply reflects the difficulty in determining the  $B^F$  values of these weak features (particularly in light of the decreased scatter of the flat bands of Fig. 8). This is direct confirmation of the two-dimensional electronic structure found in the off-normal bandmapping experiment.<sup>1</sup> As discussed in that paper, if the contribution of the Cu(001) surface is neglected, then the dominant symmetry of the potential will be  $C_{6v}$  at 1 ML. Also as described in Ref. 1, a single

group analysis is appropriate. The features observed are attributed to the  $A_1(C_{6v})d_{3z^2-r^2}$  state ( $B^F=4.2$  eV), the spin-orbit-split  $E_1(C_{6v})d_{xz,yz}$  ( $B^F=4.8$  eV), and the  $A_1(C_{6v})_s$  state ( $B^F=6.3$  eV). Weak features near  $B^F=3.5, 5.2,$  and  $8$  eV are observed in some of the spectra. These are due to transitions of the underlying Cu(001) substrate. The symmetry forbidden transition originating from the silver  $E_2(C_{6v})d_{xy,x^2-y^2}$  state is not observed.<sup>1</sup>

*Two monolayers.* At 2 ML (Fig. 8),  $C_{3v}$  symmetry would be present. Experimentally, the bands are still observed to be flat and qualitatively the same as for 1 ML, except that the lowest band (greatest  $B^F$ ) has shifted from  $B^F=6.4$  eV at 1 ML to  $6.7$  eV at 2 ML. This may be a manifestation of density-of-states (DOS) broadening in going from two- to three-dimensionality, since bandwidth should increase with slab thickness.<sup>3</sup>

Under  $C_{3v}$  symmetry, the representations and selection rules are only slightly different, with the above-mentioned states essentially the same. Operating under  $C_{6v}$  selection rules, the transition from the  $E_2$  state is forbidden. In going from 1 to 2 ML, this  $E_2(C_{6v})$  state becomes  $E(C_{3v})$ , which is symmetry allowed. A weak feature near  $B^F=5.4$  eV is seen at some photon energies at coverages of 1 and 2 ML, but it is believed to be due to the tail of the Cu(001) feature at  $B^F=5.2$  eV. From the off-normal study,<sup>1</sup> it is known that the  $E_2$  state should be in this region of  $B^F$ . Perhaps it is obscured by the copper peak or the  $C_{6v}$  contribution to the  $C_{3v}$  potential dominates it to the extent that the transition is still essentially forbidden. [ $\mathbf{A} \cdot \mathbf{p}$  vectorial alignment also militates against a large partial cross section at normal emission, since it is only allowed for the in-surface-plane component of the polarization,  $\mathbf{A}_{\parallel}$ . However the same is true for the  $E_1(d_{xz,yz})$  state, which nonetheless has significant intensity.]

The features near  $B^F=4.7$  and  $4.9$  eV at 1 and 2 ML are assigned as the spin-orbit-split doublet of the  $Y_2^{\pm 1}[E_1(C_{6v})$  or  $E(C_{3v})]$  state. The observed splitting and rms scatter at 1 ML is  $0.26 \pm 0.05$  eV, and at 2 ML it is  $0.25 \pm 0.04$  eV. These values agree well with that of  $0.24$  eV found in the resonance lamp experiment for coverages near 1 ML.<sup>1</sup>

*Three monolayers.* At 3 ML (Fig. 9), qualitatively new behavior is observed. For all adlayers thicker than 2 ML, there will always be a  $C_{3v}$  symmetry interface layer and a  $C_{3v}$  symmetry surface layer sandwiching octahedral symmetry layers between them. This is assuming a layer-by-layer and face-centered-cubic growth pattern. At 3 ML, the first octahedral layer will be present and experimentally two new bands are observed. We associate these with transitions allowed under double group, perturbed octahedral selection rules.<sup>1</sup> One, near  $B^F=5.5$  eV, overlaps with the copper substrate feature but is much stronger than before. The other, at  $B^F=6.1$  eV, has no substrate complications. Moreover, the band structure at 3 ML is distinctly bulklike in that there are now six separate levels between  $B^F=4.0$  eV and  $B^F=7.0$  eV, corresponding to bands 1–6 of Ag(111) (Fig. 12). There may also be the beginning of dispersion in bands  $d$  and  $e$  at  $h\nu \leq 20$  eV.

It may be that the feature at  $B^F=4.2$  eV is not merely a precursor of one of the bulk bands but also develops into

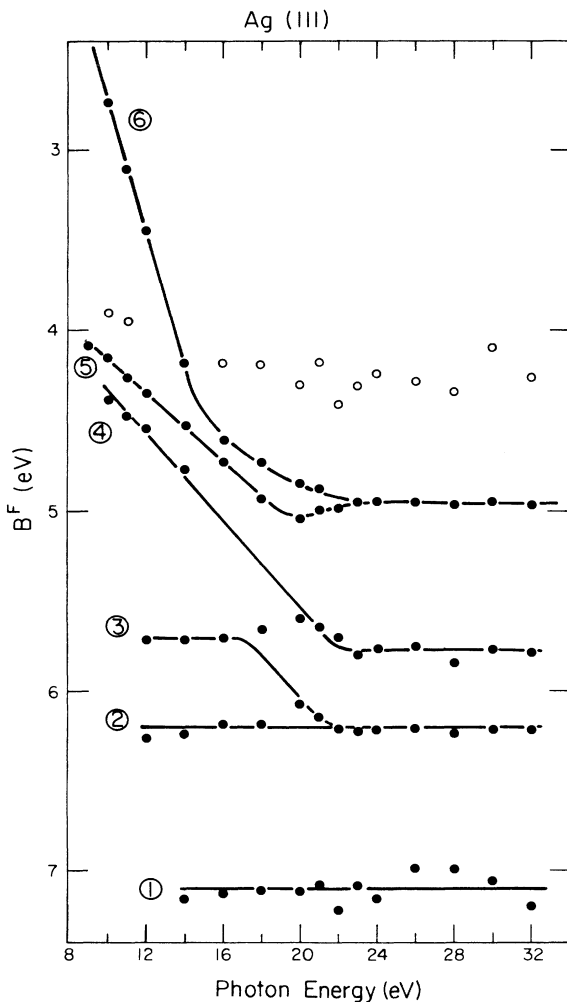


FIG. 12. Same as Fig. 7 but for Ag(111).

a residual  $A_1(C_{3v})$  state of the surface layer, and possibly of the interface layer as well. This could explain the shoulder (open circles in Figs. 11 and 12) seen near 4 eV in the bulk Ag(111) spectra, previously interpreted as being due to indirect transitions.<sup>9</sup> At  $h\nu=22-32$  eV, this feature can be seen to persist as a separate peak even up to 4 ML, where it finally becomes enveloped in the broadening bands  $d$  and  $e$ .

A peak at  $B^F=3.5$  eV is seen at  $h\nu=10-16$  eV at coverages of 3–5 ML. It appears to be due to the copper substrate spectral structure, but it may also be a precursor to the dispersive  $s$ - $p$  band away from the bulk zone center.

The success of the group theoretical analysis in explaining the new bands at 3 ML is the strongest evidence to date that the growth mode is layer by layer beyond 1 ML, at least up to coverages of 3 ML. Considering that only 100–200 atoms are necessary to observe bulklike effects in Au and Ag clusters,<sup>10,11</sup> the absence of any other bands at 1- and 2-ML coverages is strongly suggestive of a planar nature, and supports the hypothesis of continued layer-by-layer growth.

*Four and Five Monolayers.* Continuing to the 4- and 5-ML coverages (Figs. 10 and 11), the bands generally remain stationary at  $h\nu \geq 26$  eV. However, dispersion is observed in bands  $d$  and  $e$  as the photon energy decreases to 10 eV. This mimics what is observed for Ag(111) in Fig. 12 and corresponds to the dispersion occurring away from  $\Gamma$  ( $h\nu \sim 24$  eV) and toward  $L$  ( $h\nu < 6$  eV) in the bulk three-dimensional Brillouin zone.<sup>12</sup> The appearance of states near  $B^F=3.5$  eV may be related to the dispersion of the bulk band 6 up to the Fermi energy near the  $L$  point. But regardless of that assignment, the features near  $B^F=4.7$  eV dispersing steadily in going from  $h\nu=20$  to 10 eV in the 4–5 ML systems. Note that in the 5-ML case, the assignments in bands  $d$ ,  $e$ , and  $f$  have been changed to be consistent with bands 4, 5, and 6 of Ag(111). This is justified in part by the similarity of the 5-ML and Ag(111) spectra.

The gradual, continuous development toward bulk band structure is consistent with a layer-by-layer growth pattern. At the 5-ML exposure, there are approximately  $6 \times 10^{15}$  atoms of Ag per square centimeter and a 5-ML slab would be approximately 13 Å thick. At  $5 \times 10^{15}$  atoms/cm<sup>2</sup>, the electronic density of states of the Au clusters studied by Lee *et al.*<sup>10</sup> is bulklike. Assuming hemispherical cluster growth, this implies that bulk behavior is associated with thicknesses or heights of 10–20 Å. In this experiment the perpendicular direction alone is being probed. If significant island formation were occurring in the silver overlayer, thicknesses of twice or more relative to that calculated for the quoted silver exposure could well be expected and the transition from two- to three-dimensionality would be much more rapid. Also, the continued observation of the  $A_1(C_{3v})$  state at  $B^F=4.3$  eV suggests the existence of large sections of an intact hexagonal topmost layer.

Let us now consider the absence from the overlayer spectra of an intense, sharp feature for band 6 at  $B^F < 4$  eV. The only silver overlayer features near the energy of the Ag(111) band 6 at  $h\nu < 14$  eV are the weak, flat structure at  $B^F=3.5$  eV and the broad, intense precursor to the

Ag(111) surface state near  $E_F$ . At the other extreme, sharp, intense silver overlayer peaks are seen for  $h\nu \geq 14$  eV at  $B^F \geq 4$  eV.

The most likely cause of the observed behavior is that interactions with the substrate affect band 6. Band 6 at  $B^F < 4$  eV and the Ag(111) surface state are of  $s$ - $p$  character, while bands 1–6 of Ag(111) at  $B^F \geq 4$  eV are mainly of  $d$  character. It appears that adsorbate  $d$  levels can sometimes behave as isolated core states and not participate in interactions with the substrate.<sup>1</sup> On the other hand, delocalized  $s$  and  $p$  electrons would be the most likely candidates for interaction with the substrate. Hence, substrate-adsorbate bonding interactions, which must be occurring to some extent, based on the observed stability of the overlayer on the Cu(001) surface, would not perturb the adsorbate  $d$  levels ( $B^F \geq 4$  eV). Rather they would severely affect the  $sp$  states; e.g., band 6 at  $B^F < 4$  eV and the surface state. Note that if all  $sp$  states were thus affected, it would preclude hybridization between the  $d$  bands and the  $sp$  band.

#### B. Development of Ag(111) spectral characteristics

Besides the development of normal emission dispersion, several other facets of spectral behavior peculiar to Ag(111) develop in the  $c(10 \times 2)$ Ag overlayers.

*Band 7 resonance.* A sharp variation in the intensities of the  $d$ -band peaks is observed in Ag(111) through the range  $h\nu=21-24$  eV. It is caused by the matching of the photon energy and the energy separation between the initial state  $d$  bands and a flat region of band 7 near  $\Gamma$ , the center of the bulk Brillouin zone. This is also observed at 4- and 5-ML coverages in  $c(10 \times 2)$ Ag.

While it is extremely difficult to fit each peak accurately, it is possible to measure the intensities of the top and bottom halves of the Ag valence band (VB). Figure 13 shows a comparison of these integrated intensities for Ag(111) (Ref. 5) and  $c(10 \times 2)$ Ag/Cu(001). It is obvious that the cross-section resonance seen in Ag(111) is also occurring in the adlayers, although to a diminished degree. Qualitatively, the resonance is observable in the raw spectra for the above systems from  $h\nu=20$  eV to  $h\nu=26$  eV.

This behavior occurs in Ag(111) at  $\Gamma$ , where atomic effects should dominate. Atomic Ag spectra<sup>13</sup> do show a distinct increase in cross-section magnitude over the energy range  $h\nu=17-20$  eV. The results over the range of  $h\nu=20-27$  eV are too incomplete to dismiss the possibility of an atomic cross-section resonance occurring there. However, the resonance is not observed at the lower exposures of the  $c(10 \times 2)$ Ag system and the effect is seen to grow stronger with increasing exposure.

*Constant kinetic energy feature.* Another feature identified with Ag(111) is the constant kinetic energy peak at 17 eV with respect to the Fermi level. This is also due to the flat region of band 7 of Ag(111), near the center of the bulk Brillouin zone. Electrons scatter into it, producing a peak that appears to move across the spectra at  $B^F=h\nu-17$  eV for  $h\nu=26-32$  eV.<sup>9</sup> At 28 and 30 eV photon energies (Figs. 5 and 6), this feature is observable at 4 and 5 ML and at  $h\nu=32$  eV at 5 ML. This is a

TABLE II. Comparison of the binding energies with respect to the Fermi energy and the full widths at half maximum (FWHM) of the Ag(111) surface state and its precursor observed in  $c(10\times 2)\text{Ag}/\text{Cu}(001)$ . All overlayer measurements were derived from data collected at normal emission for  $h\nu=8\text{ eV}$ . The Ag(111) data is from Refs. 5 and 7.

Monolayers of $c(10\times 2)\text{Ag}/\text{Cu}(001)$	Ag(111)	$B^F$ (eV)	Width (eV)
		$0.065\pm 0.004$	$0.111\pm 0.007$
5		0.10	0.7
4		0.11	1.0
3		0.14	1.2
2		0.11	1.4

strong indication of bulklike final-state behavior in the silver overlayer.

*Surface state.* At lower photon energies,  $h\nu=6-12\text{ eV}$ , the Ag(111) surface state is present near the Fermi level. At some of these photon energies, copper features obscure this spectral region but for  $h\nu=7-9\text{ eV}$  the development of a precursor surface state is easily seen. Table II contains a summary of surface-state data taken from the  $h\nu=8\text{-eV}$  spectra. (The  $h\nu=8\text{-eV}$  spectra have a flat Cu substrate background.) The binding energies were determined by visual inspection. The widths were found by fitting the Fermi edge step and surface peak with a Gaussian step and Lorentzian peak function multiplied by a Fermi occupation function ( $T=300\text{ K}$ ).<sup>14</sup> The Gaussian step

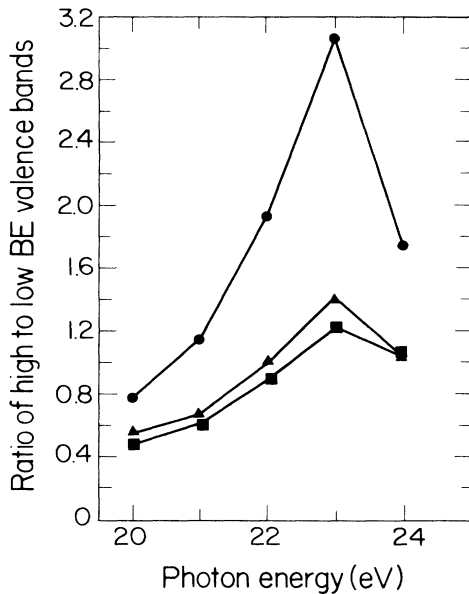


FIG. 13. The ratio of the intensity of the high  $B^F$  half of the silver valence bands to the intensity of the low  $B^F$  half of the silver bands, plotted as a function of photon energy for the samples Ag(111), solid circles, and 5, solid triangles, and 4-ML solid squares, of  $c(10\times 2)\text{Ag}/\text{Cu}(001)$ . The ratio of the 5-ML values (including the rms deviation) to the Ag(111) values is  $0.57\pm 0.09$ . The ratio of the 4-ML values to the Ag(111) values is  $0.52\pm 0.09$  and to the 5-ML values is  $0.92\pm 0.07$ .

and occupation function were set to the value of the Fermi energy determined by visual inspection and the Lorentzian mean was set to the peak energy, also found by visual inspection. The listed widths are the FWHM of the unabridged Lorentzians. Instrumental broadening is insignificant compared to these widths. [The Ag(111) values were taken from Ref. 7. The peak positions were determined visually and the peak width is a result of Gaussian fittings corrected for instrumental broadening. The data range was  $h\nu=6-12\text{ eV}$ . Fitting the Ag(111)  $h\nu=8\text{-eV}$  spectrum with the functions used on the overlayer spectra produced values consistent with these.] Also, despite the obstruction of substrate peaks, the  $B^F$  values of the overlayer peak determined at nearby photon energies were consistent with those from  $h\nu=8\text{ eV}$ . The state has roughly the same binding energy as for Ag(111) but is much wider owing to the asymmetric tail on the higher binding energy side. This may be due to interaction between the adsorbate and substrate.

At 3- and 5-ML coverages, the angular dependence of the precursor surface state was investigated at  $h\nu=8\text{ eV}$ . All spectra were taken with the same parameters as shown in Fig. 1, save that the angle-resolved photoemission spectroscopy (ARPES) analyzer was rotated off normal to obtain nonzero values of  $k_{||}$ , the parallel component of crystal momentum. While no clean Cu(001) substrate off-normal spectra were available for direct comparison, the general appearance of the adsorbate spectra remained much the same, and the intensity of the precursor state was estimated by linearly extrapolating the diminishing background back up to the Fermi edge.

At 3 ML, rotating in the  $\bar{\Gamma}-\bar{T}-\bar{K}$  plane above and below the light polarization, the state was evident at  $\theta_e=\pm 2^\circ$  ( $k_{||}=\pm 0.032\text{ \AA}^{-1}$ ) and at  $\theta_e=\pm 5^\circ$  ( $k_{||}=\pm 0.079\text{ \AA}^{-1}$ ). In the  $\bar{\Gamma}-\bar{\Sigma}-\bar{M}$  plane, the state was present at  $\theta_e=\pm 2^\circ$ ,  $\pm 5^\circ$ , and  $\pm 10^\circ$  ( $k_{||}=\pm 0.158\text{ \AA}^{-1}$ ), both toward and away from the light polarization. Rotating the analyzer in the  $\bar{\Gamma}-\bar{\Sigma}-\bar{M}$  plane toward the polarization of the synchrotron radiation ( $\theta_e > 0$ ), at  $\theta_e=15^\circ$  ( $k_{||}=0.236\text{ \AA}^{-1}$ ) the precursor peak disappeared. At  $\theta_e=20^\circ$  ( $k_{||}=0.312\text{ \AA}^{-1}$ ), the peak reappeared. Within the precision of our measurements, the state does not appear to be dispersing as a function of  $k_{||}$ . At a coverage of 5 ML, rotating in the  $\bar{\Gamma}-\bar{\Sigma}-\bar{M}$  plane and toward the light polarization, the state was present at  $\theta_e=0^\circ$  and  $2^\circ$  but not at  $5^\circ$ . Again, there

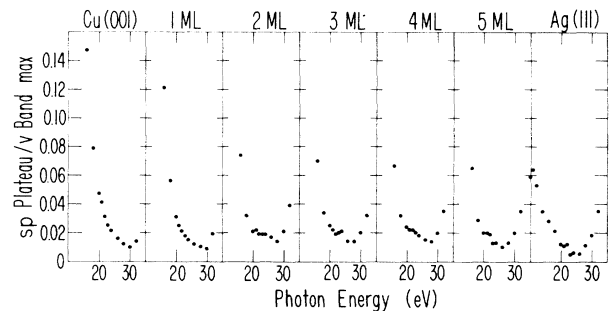


FIG. 14. The ratio of the  $sp$  plateau height to the valence-band maximum, vs photon energy, for Cu(001), 1, 2, 3, 4, and 5 ML of  $c(10\times 2)\text{Ag}/\text{Cu}(001)$ , and Ag(111).

seems to be no dispersion with  $k_{\parallel}$ .

The behavior at 5 ML is consistent with that observed by Hansson and Flodstrom<sup>15</sup> in Ag(111) at  $h\nu=10.2$  eV ( $k_{\parallel}<0.103$  Å<sup>-1</sup>). However, the 3-ML precursor seems to extend much further in  $k_{\parallel}$  space. It appears that the precursor state may be restricted to a smaller area of the two-dimensional surface Brillouin zone as the overlayer becomes thicker and the valence bands become more three-dimensional.

Since our initial report<sup>4</sup> on such a precursor surface state, it has been observed in other Ag overlayer systems.<sup>16,17</sup> Variations in the overlayer electronic structure with substrate,<sup>17</sup> particularly those states with strong *sp* character, is not unexpected. In the case of Ag overlayers on Si(111),<sup>16</sup> the authors claim to observe a series of *sp* surface states of varying number and energy separation, due to spatial localization induced by the thin film. In comparison to this work, their coverages are larger than those used here and the weaker peaks at larger binding energies would be obscured by the strong bulk Cu *d* bands.

*sp plateau.* The ratio of the *sp* plateau height to the valence-band intensity is dependent upon the valence electronic structure of the system as discussed in Refs. 5 and 9. (In Ref. 7, it has been empirically shown that either the valence-band maximum or integrated intensity can be used for this comparison.) The indirect transitions contributing to the *sp* plateau intensity are dependent upon the position of the bands near  $E_F$ , e.g., band 6 of Ag(111). Figure 14 shows this ratio versus photon energy for clean Cu(001), 1–5 ML of  $c(10\times 2)\text{Ag}/\text{Cu}(001)$ , and Ag(111). As the exposure is increased, the behavior of the ratio moves slowly toward that of Ag(111). This is yet another indication of the development of Ag(111)-like behavior in the metal overlayer. This specifically suggests that band 6 is “slowly” developing in the silver overlayers, delayed by the hypothesized interaction of the *sp* states with the Cu(001) substrate.

*Spectral appearance.* Finally, it is of interest to note the significant similarities between the spectra of Ag(111) and those of 5-ML  $c(10\times 2)\text{Ag}/\text{Cu}(001)$ . As an example, those at 24 eV (Fig. 4) bear a striking resemblance if the Cu features are neglected. Qualitatively, this is strong evidence for the approach of the valence structure of the  $c(10\times 2)\text{Ag}$  system toward that of bulk Ag(111).

## V. CONCLUSIONS

Based upon the results of the LEED-AES calibration of Ref. 1 and the previous work discussed therein, the  $c(10\times 2)\text{Ag}/\text{Cu}(001)$  adlayer is assumed to be geometrically two-dimensional at coverages near 1 ML. It has been shown in the off-normal angle-resolved photoemission experiment of Ref. 1 that the monolayer *d*-band structure is also electronically two-dimensional. Here, conclusive evidence is presented to document the development of the valence bands of the  $c(10\times 2)\text{Ag}$  from a two-dimensional to a three-dimensional electronic structure.<sup>18</sup> The 3-ML results demonstrate the importance of developing a crystal field similar to that of the bulk. Higher coverages are necessary to acquire sufficient

periodicity in real space to observe dispersion in the third dimension. By a coverage of 5 ML, the spectral behavior of the overlayer valence (and conduction) bands is very similar to that of Ag(111). This includes dispersion as a function of  $k_{\perp}$ , the band 7 resonance, the constant kinetic energy feature, the Ag(111)-like surface state, the *sp*-plateau intensity profile, and, finally, the detailed visual appearance of the spectra themselves.

## ACKNOWLEDGMENTS

This work was supported by the Director, Office of Energy Research, Office of Basic Energy Sciences, Chemical Sciences Division of the U.S. Department of Energy under Contract No. DE-AC03-76SF00098. It was performed at the Stanford Synchrotron Radiation Laboratory, which is supported by the Department of Energy's Office of Basic Energy Sciences. J. G. Tobin acknowledges support by the National Science Foundation. We also wish to acknowledge Mrs. Winifred Heppler for the preparation of the copper crystal and D. J. Trevor, C. C. Bahr, and J. J. Barton for their programs used in data reduction. Discussions with R. F. Davis and M. G. Mason were enlightening and greatly appreciated.

## APPENDIX

We describe here a model for Ag-adsorbate–Cu-substrate photoemission ratios assuming a layer-by-layer growth pattern.<sup>19</sup> For the substrate,

$$i_{\text{Cu}} = i_{\text{Cu}}^0 e^{-z/z_0}, \quad (\text{A1})$$

where  $i_{\text{Cu}}$  is the photoemission intensity of the copper features including attenuation from the overlayer,  $i_{\text{Cu}}^0$  is the photoemission intensity of the clean copper, bulk Cu(001),  $z$  the overlayer thickness, and  $z_0$  the escape depth of the substrate photoelectrons, through the adsorbate. Note that there is no correction for light attenuation. For the adsorbate,

$$j_{\text{Ag}} = \sum_{k=1}^n j_{\text{Ag}}^k, \quad (\text{A2})$$

where  $j_{\text{Ag}}$  is the photoemission intensity from the silver overlayer,  $j_{\text{Ag}}^k$  is the photoemission intensity from the  $k$ th monolayer of an overlayer slab  $n$  monolayers thick, given by

$$j_{\text{Ag}}^k = j_{\text{Ag}}^1 e^{-(k-1)t/t_0}, \quad (\text{A3})$$

where  $j_{\text{Ag}}^1$  is the photoemission intensity from the topmost monolayer of the overlayer,  $k=1$ ,  $t$  is the thickness of one monolayer,  $(k-1)t$  is the thickness of the overlayer above the  $k$ th monolayer,  $t_0$  is the escape depth of the adsorbate electrons, through the adsorbate.

Note that

$$z = nt. \quad (\text{A4})$$

The photoemission ratio is given by

$$R_n = \frac{j_{Ag}}{i_{Cu}} = \frac{j_{Ag}^1}{i_{Cu}^0} \sum_{k=1}^n \frac{e^{-(k-1)t/t_0}}{e^{-z/z_0}}. \quad (A5)$$

In the case of an overlayer only 1 ML thick:  $k = n = 1$ ,  $z = t$

$$R_1 = \frac{j_{Ag}^1}{i_{Cu}^0} \frac{1}{e^{-t/z_0}}. \quad (A6)$$

Defining a ratio normalized to the ratio at 1 ML:

$$R'_n = \frac{R_n}{R_1} = \sum_{k=1}^n \frac{(e^{-(k-1)t/t_0})(e^{z/z_0})}{e^{t/z_0}}. \quad (A7)$$

Substituting  $z = nt$  and setting  $t_0 = z_0$  (same kinetic energy range<sup>20</sup>)

$$R'_n = \sum_{k=1}^n \frac{e^{-(k-1)t/z_0}}{e^{-(n-1)t/z_0}}. \quad (A8)$$

Equation (A8) was used to calculate the theoretical values of Table II.

\*Present address: Department of Chemistry, University of Wisconsin, Madison, Wisconsin 53706.

†Present address: IBM Thomas J. Watson Research Center, Yorktown Heights, NY 10598.

‡Present address: National Bureau of Standards, B206/220, Gaithersburg, Maryland 20899.

<sup>1</sup>J. G. Tobin, S. W. Robey, and D. A. Shirley, *Phys. Rev. B* **33**, 2270 (1986), and references therein. This article contains a rather extensive listing of pertinent studies.

<sup>2</sup>P. Heimann, H. Neddermeyer, and H. F. Roloff, *Proceedings of the 7th International Vacuum Congress and the Third International Conference on Solid Surfaces*, Vienna, Austria, 1977 (unpublished).

<sup>3</sup>F. J. Arlinghaus, J. G. Gay, and J. R. Smith, *Phys. Rev. B* **20**, 1332 (1979); **25**, 643 (1982).

<sup>4</sup>J. G. Tobin, S. W. Robey, L. E. Klebanoff, and D. A. Shirley, *Phys. Rev. B* **28**, 6169 (1983).

<sup>5</sup>J. G. Nelson, S. Kim, W. J. Gignac, R. S. Williams, J. G. Tobin, S. W. Robey, and D. A. Shirley, *Phys. Rev. B* **32**, 3465 (1985).

<sup>6</sup>S. D. Kevan and D. A. Shirley, *Phys. Rev. B* **22**, 542 (1980).

<sup>7</sup>J. G. Tobin, Ph.D. thesis, University of California, Berkeley, 1983.

<sup>8</sup>D. P. Spears, R. Melander, L. G. Petersson, and S. B. M. Hagstrom, *Phys. Rev. B* **21**, 1462 (1980).

<sup>9</sup>P. S. Wehner, R. S. Williams, S. D. Kevan, D. Denley, and D. A. Shirley, *Phys. Rev. B* **19**, 6164 (1979).

<sup>10</sup>S.-T. Lee, G. Apai, M. G. Mason, R. Benbow, and Z. Hurych, *Phys. Rev. B* **23**, 505 (1981).

<sup>11</sup>G. Apai, S.-T. Lee, and M. G. Mason, *Solid State Commun.* **37**, 212 (1981).

<sup>12</sup>The deviations from linearity in Figs. 7, 8, and 9 are reasonably random. For example, they could be due to imprecisions caused by the changes in the ratio of adsorbate to substrate signal. Also, some of the peaks are weak at lower coverages and their centers could only be determined relatively imprecisely. The dispersion in Fig. 10 is at the location predicted upon the basis of the dispersion in bulk Ag(111) in Fig. 11. We are thus distinguishing between random noise and systematic and predicted deviation from horizontal linearity.

<sup>13</sup>M. O. Krause, P. R. Woodruff, and T. A. Carlson, *J. Phys. B* **14**, L673 (1981); M. O. Krause, *J. Chem. Phys.* **72**, 6474 (1980).

<sup>14</sup>A. Gaussian step function is an integrated Gaussian peak. It serves to fit the jump in intensities at the Fermi edge. The Lorentzian with the Fermi occupation function is used to fit the surface state itself.

<sup>15</sup>G. V. Hansson and S. A. Flodstrom, *Phys. Rev. B* **17**, 473 (1978).

<sup>16</sup>A. L. Wachs, A. P. Shapiro, T. C. Hsieh, and T. C. Chiang, *Phys. Rev. B* **33**, 1460 (1986).

<sup>17</sup>A. P. Shapiro, A. L. Wachs, T. C. Hsieh, T. Miller, P. John, and T. C. Chiang, *Phys. Rev. B* **34**, 7425 (1986).

<sup>18</sup>This has subsequently been observed in other systems as well. For example, see T. W. Capehart, *Bull. Am. Phys. Soc.* **31**, 265 (1986) and J. G. Tobin, J. C. Hansen, B. J. Knapp, and J. A. Benson, *ibid.* **32**, 817 (1987).

<sup>19</sup>G. Ertl and J. Koppers, *Low Energy Electrons and Surface Chemistry* (Chemie-Verlag, Weinheim, 1974), pp. 39 and 40.

<sup>20</sup>P. S. Wehner, Ph.D. thesis, University of California, Berkeley, 1978; C. R. Brundle, *J. Vac. Sci. Technol.* **11**, 212 (1974).